Harding Lawson Associates
Diablo Canyon Power Plant
ASW Bypass 10183.ASWCALC

CALCULATION COVER SHEET (LIQUEFACTION ANALYSIS)

File Number _____
Calculation Number: 10183-96-02
Number of pages: 27
Date 7/18/96
Sheet 1 of 27

Preliminary _____
Final X

PROJECT: Diablo Canyon ASW Bypass

This calculation set documents HLA's liquefaction analysis for medium dense cohesionless fill materials below the water table encountered in borings drilled on or near the ASW bypass alignment. The calculation evaluates the potential for liquefaction at various peak ground accelerations (PGAs) using procedures developed by Seed et al. (1985). The volumetric strain and settlement within the soil layer were calculated using procedures developed by Tokimatsu and Seed (1987). Ground surface settlements were estimated by HLA on the basis of the computed settlements within the liquefied soil layer, the depth of the layer, and observations by HLA and others regarding compaction methods used at the time the fill materials were placed. A residual strength was calculated for the liquefied layer using procedures developed by Seed and Harder (1990).

Preparer: _____ *date:* 7/18/96

Checker: _____ *date:* 7/18/96

Approval: _____ *date:* 7/18/96

REGISTERED PROFESSIONAL ENGINEER
WARD ANDREW HERLACHE
No. GE 002149
Exp. 3/31/99
GEOTECHNICAL
STATE OF CALIFORNIA

Approval Stamp (above)

RECORD OF REVISIONS:

Revision No.	*Date*	*Reason*	*Prepared by*	*Checked by*	*Approved by*	
0	7/18/96	ORIGINAL				

CALCULATION SHEET
Preparer: Wayne Magnusen
Checker: Robert Pyke
Date: 7/18/96

Calculation Number:10183-96-02
Revision: 0

Sheet 2 of 27

TABLE OF CONTENTS

CALCULATION SHEET
Preparer: Wayne Magnusen
Checker: Robert Pyke
Date: 7/18/96

Calculation Number:10183-96-02
Revision: 0
Sheet 3 of 27

1.0 PURPOSE:

This calculation set documents HLA's liquefaction analysis for medium dense cohesionless fill materials below the water table encountered in borings drilled on or near the ASW bypass alignment. The potential for liquefaction is evaluated and the volumetric strain and total settlement within the liquefied layer is calculated. The purpose of the calculation set is to estimate the settlement of portions of the ASW bypass piping during various seismic events.

CALCULATION SHEET
Preparer: Wayne Magnusen
Checker: Robert Pyke
Date: 7/18/96

Calculation Number:10183-96-02
Revision: 0

2.0 REFERENCES:

Harding Lawson Associates, 1996. *Geotechnical Field and Laboratory Investigation, ASW System Bypass, Units 1 & 2, Diablo Canyon Power Plant, San Luis Obispo County, California*, May 8.

Seed, H. B., K. Tokimatsu, L.F. Harder, and R.M. Chung, 1985. *Influence of SPT Procedures and Liquefaction Resistance Evaluations*, American Society of Civil Engineers, Journal of Geotechnical Engineering, Vol. 111, No. 12, December.

Tokimatsu, K. and H. B. Seed, 1987. *Evaluation of Settlement of Sands Due to Earthquake Shaking*, American Society of Civil Engineers, Journal of Geotechnical Engineering, Volume 113, No. 8, August.

PG&E References:

Mr. Al Tafoya's (of PG&E) draft memorandum entitled *Background Information of Soil Near the I.S. and for Liquefaction Issue*, dated May 31, 1996.

PG&E plan entitled *Rock Topography near ASW Bypass Piping Routing (SK-C-ASWBROCK), Revision A.*

CALCULATION SHEET
Preparer: Wayne Magnusen
Checker: Robert Pyke
Date: 7/18/96

Calculation Number:10183-96-02
Revision: 0

3.0 ASSUMPTIONS AND DESIGN INPUTS:

3.1 Subsurface Conditions

In December of 1995, HLA drilled 4 borings to characterize the backfill for purposes of the dynamic analyses of the proposed ASW Bypass being conducted by others and the slope stability evaluation being conducted by HLA. The boring locations are shown on the Site Plan, Plate 1 (see Attachment 1). The borings encountered fill that ranged in depth from 6 feet at Boring B-2 to 31-1/3 feet (the depth explored) at Boring B-4. The fill generally consisted of stiff clays and dense to very dense sands and gravel which is consistent with the 1978 borings; these materials are not believed to be susceptible to liquefaction. Unexpectedly however, two of the borings encountered medium dense sands below Mean Sea Level (Borings B-1 and B-4, see Attachments 2 and 3) as indicated by relatively low blow counts obtained during soil sampling. The relatively low blow counts occurred at a depth of 25 feet (Elevation -1 feet, Mean Sea Level), as shown the boring logs, and are in what is believed to be the original backfill placed during the CWI conduit construction. The blow count of 18 at 25 feet in Boring B-1 represents a Standard Penetration Test (SPT) N-Value (See note 1, below) and the blow count of 15 at 25 feet in Boring B-4 represents a pseudo-SPT N-value that was obtained by multiplying the field blow count by 0.7 to account for the larger sampler size (3-inch outside diameter and 2.43-inch inside diameter). For our liquefaction analyses we used the same unit weights for the cohesive and granular fills as we used in our slope stability calculations (see HLA Calculation No. 10183-96-01).

Additional details regarding the field investigation are presented in HLA's May 8, 1996 report.

---

1 The SPT N-value is defined as the number of blows of a 140-pound hammer, falling freely through a height of 30 inches, required to drive a standard split-barrel sampler (2-inch outside diameter and a 1-3/8-inch inside diameter) the final 12 inches of an 18-inch drive. For SPT procedures, see ASTM D1586.

3.1 Subsurface Conditions (continued)

The groundwater was encountered only in Boring B-4 at a depth of 24 feet (Elevation 0 feet). Because of the proximity of the site to the ocean, the groundwater level is likely influenced by tidal effects. In our liquefaction evaluation, we used a groundwater elevation of +3 feet (based on Mean Sea Level).

The zone of the medium dense sands that are located below the water table are believed to be confined to an area that is approximately 10 to 20 feet wide and 100 feet long. This zone is shown on Plate 1 (Attachment 1) and is defined by the following boundaries: the edge of the original excavation for the CWI conduit construction on the north and east, the 1980 backfill placed during repair of the electrical conduits on the west, and the clayey backfill placed during the CWI conduit and IS construction that was encountered by the 1978 Borings 4 and 5 on the south. Based on the recent Boring B-4, we have assumed that this zone is 5 feet thick, from Elevation 0 to -5 feet, throughout the zone described above. This is a conservative assumption, given that the fill was reportedly compacted to at least 95 percent relative compaction. It is more likely that the sands range from being medium dense to dense within the zone defined above.

CALCULATION SHEET
Preparer: Wayne Magnusen
Checker: Robert Pyke
Date: 7/18/96

Calculation Number:10183-96-02
Revision: 0
Sheet 7 of 27

3.2 Ground Motions

In our analyses, we evaluated the liquefaction potential for three levels of ground motion:

- A Magnitude (M, Richter Magnitude) 7-1/2 event with a peak ground acceleration (PGA) of 0.83 gravity (g)
- An M6-1/2 event with a PGA of 0.40g
- An M6 event with a PGA of 0.35g.

The larger magnitude event is believe to be representative of the maximum credible earthquake defined in the Long Term Seismic Program for the plant, while the smaller events are representative of earthquakes with higher probabilities of occurance.

CALCULATION SHEET
Preparer: Wayne Magnusen
Checker: Robert Pyke
Date: 7/18/96

Calculation Number:10183-96-02
Revision: 0

4.0 METHOD AND EQUATION SUMMARY:

The calculation evaluates liquefaction potential for using procedures developed by Seed et al. (1985). Liquefaction settlements were calculated for the design event and for lesser events using procedures developed by Tokimatsu and Seed (1987). The above referenced procedures use a dimensionless quantity called the *cyclic stress ratio* along with corrected blow counts from standard penetration tests to evaluate the potential for liquefaction and to predict liquefaction-induced settlement.

The cyclic stress ratio is defined as follows:

$$\frac{\tau_{AV}}{\sigma_o'} = 0.65 \frac{A_{MAX}}{g} \frac{\sigma_o}{\sigma_o'} r_d$$

Where,

τ_{AV}/σ_o' =cyclic stress ratio

A_{MAX} = peak ground surface acceleration (PGA) (See Section 3.2)

g = acceleration due to gravity

σ_o =total stresses at the depth under consideration

σ_o' =effective stresses at the depth under consideration

r_d =a stress reduction factor which decreases from a value of 1 at the ground surface to 0.9 at a depth of 35 feet. (we used 0.93 corresponding to a depth of 25 feet)

CALCULATION SHEET
Preparer: Wayne Magnusen
Checker: Robert Pyke
Date: 7/18/96

Calculation Number:10183-96-02
Revision: 0
Sheet 9 of 27

Blow counts are corrected using the following relation:

$$(N_1)_{60} = C_{ER} \cdot C_N \cdot N$$

where:

$(N_1)_{60}$ =corrected blow count for use with Fig. 13 (Sheet 15)

C_{ER} =correction for hammer energy; we used 1.2 for the auto-trip hammer

C_N =correction coefficient from Fig. 3(Sheet 26); we used 0.86.

N =measured blow counts (N=18 at 25 feet in B-1 using an SPT sampler. N=15 at 25 feet in B-4 is a pseudo-SPT N-value obtained by multiplying the field blow count by 0.7 to account for the larger sampler size (3-inch outside diameter and 2.43-inch inside diameter)

For the M7-1/2 event, the potential for liquefaction evaluated using Fig 13 (Sheet 15). For all three levels of ground motion, estimated strain within the liquefied layer is obtained from Fig. 6 (Sheet 18). For the lesser M6-1/2 and M6 events, the cyclic stress ratio is scaled using scaling factors of 1.19 and 1.32, respectively, as recommended by Tokimatsu and Seed (1987). Estimated settlement is calculated by multiplying the strains by the 5-foot layer thickness.

CALCULATION SHEET
Preparer: Wayne Magnusen
Checker: Robert Pyke
Date: 7/18/96

Calculation Number:10183-96-02
Revision: 0

Ground surface settlements were estimated by HLA on the basis of the computed settlements within the liquefied soil layer, the depth of the layer, and observations by HLA and others regarding compaction methods used at the time the fill materials were placed. In evaluating seismically-induced settlement, we utilized procedures developed by Tokimatsu and Seed (1987).

CALCULATION SHEET
Preparer: Wayne Magnusen
Checker: Robert Pyke
Date: 7/10/96

Calculation Number:10183-96-02
Revision: 0
Sheet 11 of 27

5.0 BODY OF CALCULATION:

CALCULATION OF TOTAL AND EFFECTIVE AT 25' DEPTH STRESSES USING DATA FROM BORINGS B-1 AND B-4 (ATTACHMENTS 2 & 3)

UNIT WEIGHTS ARE FROM HLA SLOPE STABILITY CALC. NO. 10183-96-01

B-1:

$\sigma_o' = 20(125) + 1(120) + 4(120 - 62.4)$
$= 2850$ psf

$\sigma_o = 20(125) + 5(120)$
$= 2500 + 600$
$= 3100$ psf

ESSENTIALLY THE SAME

B-2:

$\sigma_o' = 18(125) + 3(120) + 4(120 - 62.4)$
$= 2840$ psf

$\sigma_o = 18(125) + 7(120)$
$= 2250 + 840$
$= 3090$ psf

SUBSEQUENT FOR ANALYSES USE:

$\sigma_o' = 2800$
$\sigma_o = 3100$

CALCULATION SHEET
Preparer: Wayne Magnusen
Checker: Robert Pyke
Date: 7/18/96

Calculation Number:10183-96-02
Revision: 0

5.0 BODY OF CALCULATION:

CALCULATE CYCLIC STRESS RATIO FOR THE 3 MAXIMUM GROUND SURFACE ACCELERATIONS:

$$\frac{\tau_{AV}}{\sigma_o'} = 0.65 \frac{A_{MAX}}{g} \frac{\sigma_o}{\sigma_o'} \cdot r_d$$

$$= 0.65 \frac{A_{MAX}}{g} \frac{3100}{2800} 0.93$$

$$\frac{\tau_{AV}}{\sigma_o'} = 0.67 \frac{A_{MAX}}{g}$$

A_{MAX}	$\frac{\tau_{AV}}{\sigma_o'}$
0.35	0.23
0.40	0.27
0.83	0.56

CYCLIC STRESS RATIO

CALCULATION SHEET
Preparer: Wayne Magnusen
Checker: Robert Pyke
Date: 7/18/96

Calculation Number:10183-96-02
Revision: 0
Sheet 13 of 27

5.0 BODY OF CALCULATION:

BLOW COUNT CORRECTIONS:

$$(N_1)_{60} = C_{ER} \cdot C_N \cdot N$$

WHERE

N = MEASURED BLOW COUNTS
(N = 18 (BLANK B-1), N = 15 (BLANK B-4))

C_{ER} = 1.2 FOR AUTO-TRIP HAMMER

C_N = 0.86 FROM FIGURE 3 ATTACHED (ATTACHMENT No 4, SHT. 25)

$$(N_1)_{60} = 1.2(.86) \cdot N$$

$$= 1.03(N)$$

N	$(N_1)_{60}$
15	15
18	19

CALCULATION SHEET
Preparer: Wayne Magnusen
Checker: Robert Pyke
Date: 7/18/96

Calculation Number:10183-96-02
Revision: 0
Sheet 14 of 27

5.0 BODY OF CALCULATION:

EVALUATE LIQUEFACTION POTENTIAL FOR DESIGN SEISMIC EVENT

$A_{max} = 0.83g$

USE RELATIONSHIP BY SEED ET AL. (1985) PRESENTED ON FIGURE 13 RELATING CYCLIC STRESS RATIO AND $(N_1)_{60}$ VALUES TO LIMITING STRAINS FOR NATURAL DEPOSITS OF CLEAN SAND.

$$\frac{\tau_{AV}}{\sigma_o'} = 0.56$$

$$(N_1)_{60} = 15 \text{ & } 17$$

RESULTS:

POINTS PLOT WITHIN LIQUEFACTION ZONE (SEE SHEET 15)

CALCULATION SHEET
Preparer: Wayne Magnusen
Checker: Robert Pyke
Date: 7/18/96

Calculation Number:10183-96-02
Revision: 0
Sheet 15 of 27

5.0 BODY OF CALCULATION:

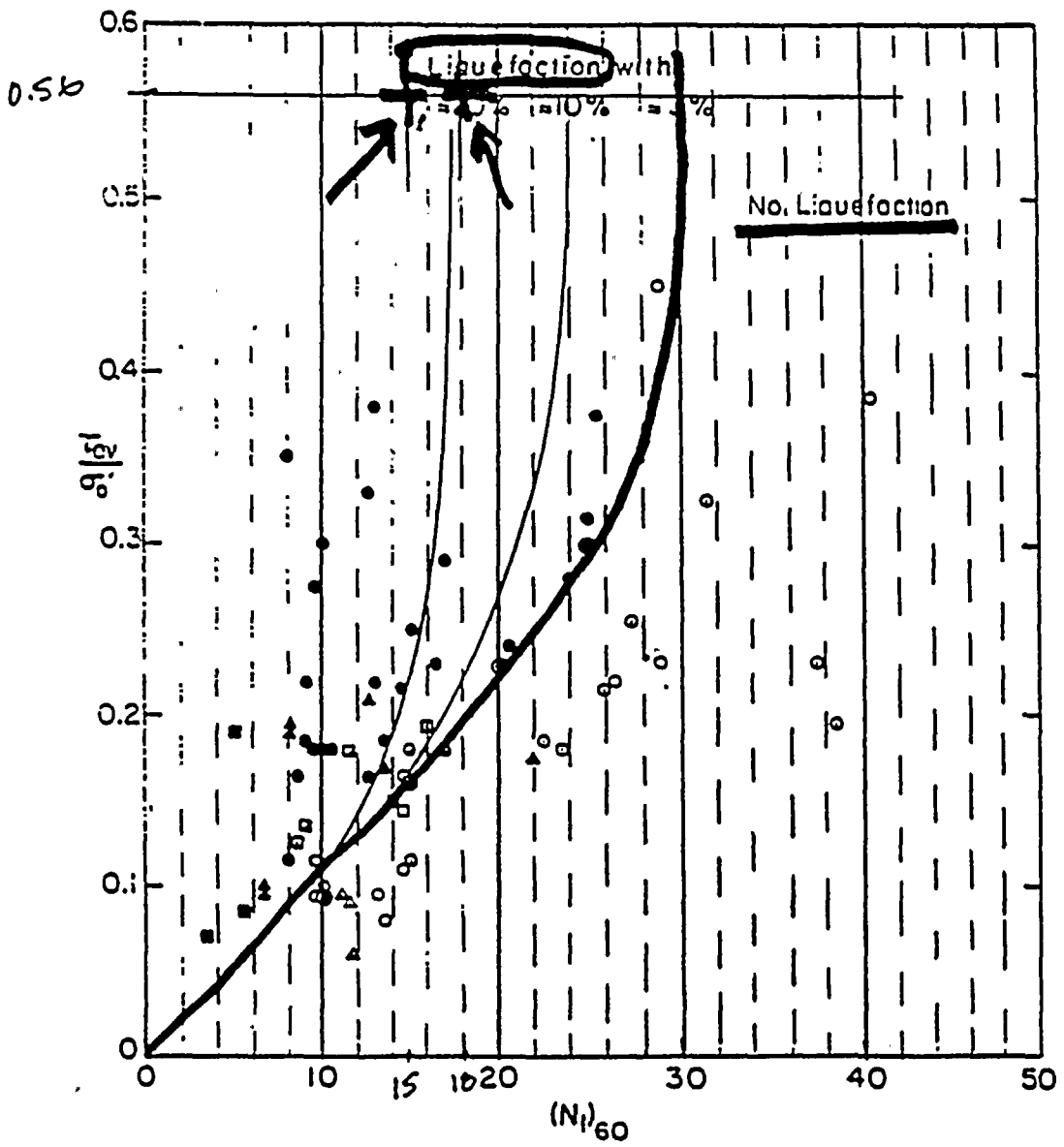

FIG. 13 TENTATIVE RELATIONSHIP BETWEEN CYCLIC STRESS RATIO, N_1-VALUES AND LIMITING STRAINS FOR NATURAL DEPOSITS OF CLEAN SAND

M = 7½

CALCULATION SHEET
Preparer: Wayne Magnusen
Checker: Robert Pyke
Date: 7/18/96

Calculation Number:10183-96-02
Revision: 0
Sheet 16 of 27

5.0 BODY OF CALCULATION:

CALCULATE SETTLEMENT

SCALING FACTORS (TOKIMATSU & SUDD, 1987)

$M = 6 \quad r_m = 1.32$

$M = 6\frac{1}{2} \quad r_m = 1.19$

$M = 7\frac{1}{2} \quad r_m = 1.00$

CALCULATE CYCLIC STRESS RATIOS USING

$$\left(\frac{\tau_{AV}}{\sigma_o'}\right)_{M=7.5} = \frac{\tau_{AV}}{\sigma_o'} \times \frac{1}{r_m}$$

M	A_{MAX}	$\frac{\tau_{AV}}{\sigma_o'}$	$\left(\frac{\tau_{AV}}{\sigma_o'}\right)_{M=7.5}$
6	0.35	0.23	0.17
$6\frac{1}{2}$	0.40	0.27	0.23
$7\frac{1}{2}$	0.83	0.56	0.56

CALCULATION SHEET
Preparer: Wayne Magnusen
Checker: Robert Pyke
Date: 7/18/96

Calculation Number:10183-96-02
Revision: 0
Sheet 17 of 27

5.0 BODY OF CALCULATION:

ENTER FIGURE 6 (SHEET 18)
TO OBTAIN ESTIMATED VOLUMETRIC STRAIN

M	STRAIN FOR $(N_1)_{60}=15$	STRAIN FOR $(N_1)_{60}=19$
6	1.1	0.1
6 1/2	1.9	1.1
7 1/2	1.9	1.5

FOR A 5-FOOT (60-INCH) LAYER

M	SETTLEMENT (INCHES) FOR $(N_1)_{60}=15$	FOR $(N_1)_{60}=19$
6	0.66	0.06"
6 1/2	1.14	0.66
7 1/2	1.14	0.90

CALCULATION SHEET
Preparer: Wayne Magnusen
Checker: Robert Pyke
Date: 7/18/96

Calculation Number:10183-96-02
Revision: 0
Sheet 18 of 27

5.0 BODY OF CALCULATION:

M=7½ 0.56

M=6½ 0.23

M=6 0.17

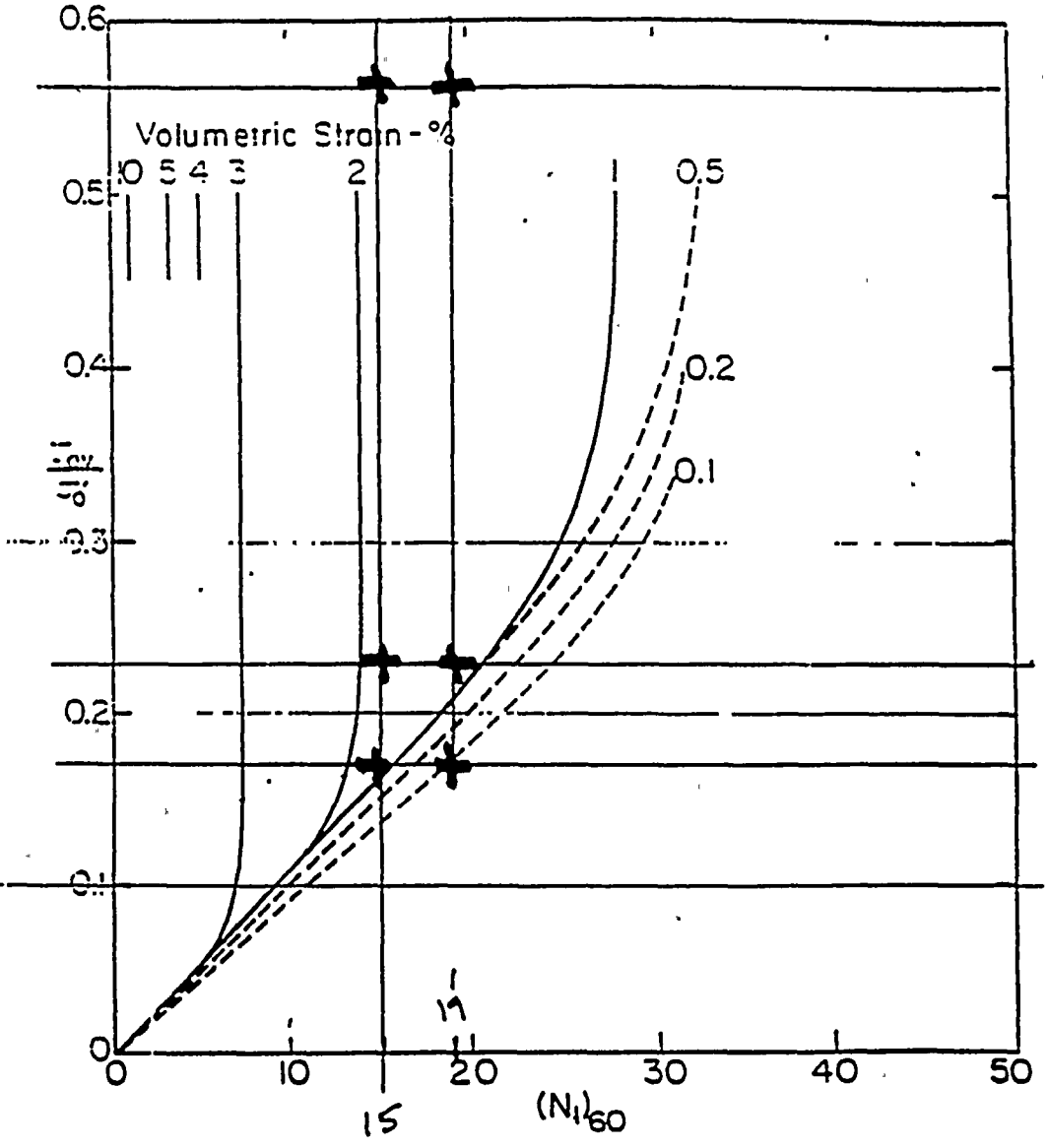

FIG. 6 PROPOSED RELATIONSHIP BETWEEN CYCLIC STRESS RATIO, $(N_1)_{60}$ AND VOLUMETRIC STRAIN FOR SATURATED CLEAN SANDS

M 7½

CALCULATION SHEET
Preparer: Wayne Magnusen
Checker: Robert Pyke
Date: 7/10/96

Calculation Number:10183-96-02
Revision: 0

6.0 RESULTS AND CONCLUSIONS:

6.1 Liquefaction Potential

Our analyses indicates that there is a high probability of liquefaction for the medium dense sands located below the water table during the M7-1/2 event. For the M6 event, the data points plot near the border between "liquefaction" and "no liquefaction" indicating that there is a much lower chance of liquefaction occurring during the smaller event.

6.2 Seismically-induced Settlement

For the M7-1/2 event (PGA of 0.83g), the computed maximum settlement of the 5-foot layer that liquefies is approximately 1 inch. Because of the depth of this layer and the limited extent of the medium dense sands, we judged that the maximum ground surface settlements could be up to approximately 50 percent of the computed settlements. This would result in a maximum ground surface settlement on the order of 1/2 inch during the M7-1/2 event. For the M6 event (PGA of 0.35g), the computed maximum settlement of the 5-foot layer that liquefies is approximately 1/2 inch. As with the larger event, we judge that the maximum ground surface settlement will be approximately 50 percent of the computed value; approximately 1/4 inch.

CALCULATION SHEET
Preparer: Wayne Magnusen
Checker: Robert Pyke
Date: 7\10\96

Calculation Number:10183-96-02
Revision: 0

Differential settlement of the proposed ASW Bypass could occur during an earthquake because the proposed pipelines will cross over the zone of medium dense sands. We judge that the magnitude of the maximum differential settlement will be approximately equal to the maximum ground surface settlements mentioned above. Because of the depth of the sands, the differential settlement will not occur abruptly, but will occur gradually along the pipeline. For design purposes, we recommend assuming that the estimated maximum differential settlement occurs over a distance of 25 feet.

The settlements mentioned above are the result of densification of the sands following dissipation of pore water pressures developed as a result of seismic shaking. Therefore, the settlements will take place following the earthquake as pore water pressures are allowed to dissipate. As a result, these settlements should not be added to the transient displacements that are predicted for the pipelines during the earthquake shaking.

These estimated settlements are maximum values that could occur during a single event. It is possible for liquefaction to occur during an earthquake, but to have little or no observable settlement; this does not mean that settlement will not occur during future earthquakes. While liquefaction has been observed to occur repeatedly at the same site during multiple earthquake, the settlement estimates represent the upper bound of accumulative settlement during repeated events at any given point at the site.

CALCULATION SHEET
Preparer: Wayne Magnusen
Checker: Robert Pyke
Date: 7/18/96

Calculation Number:10183-96-02
Revision: 0

We judge the risk of lateral movements due to liquefaction to be very low because of the discontinuous nature of the medium dense sands and the fact that they are confined on all sides.

ATTACHMENTS:

1. Site Plan, Plate 1 (Sheet 22)
2. Log of Boring B-1, Plate 2 (Sheet 23)
3. Log of Boring B-4, Plate 3 (Sheet 24)
4. Figure 3 (Tokimatsu and Seed, 1987) (Sheet 25)
5. Figure 13 (Seed et al. 1985) (Sheet 26)
6. Figure 6 (Tokimatsu and Seed, 1987) (Sheet 27)

ATTACHMENT NO.1

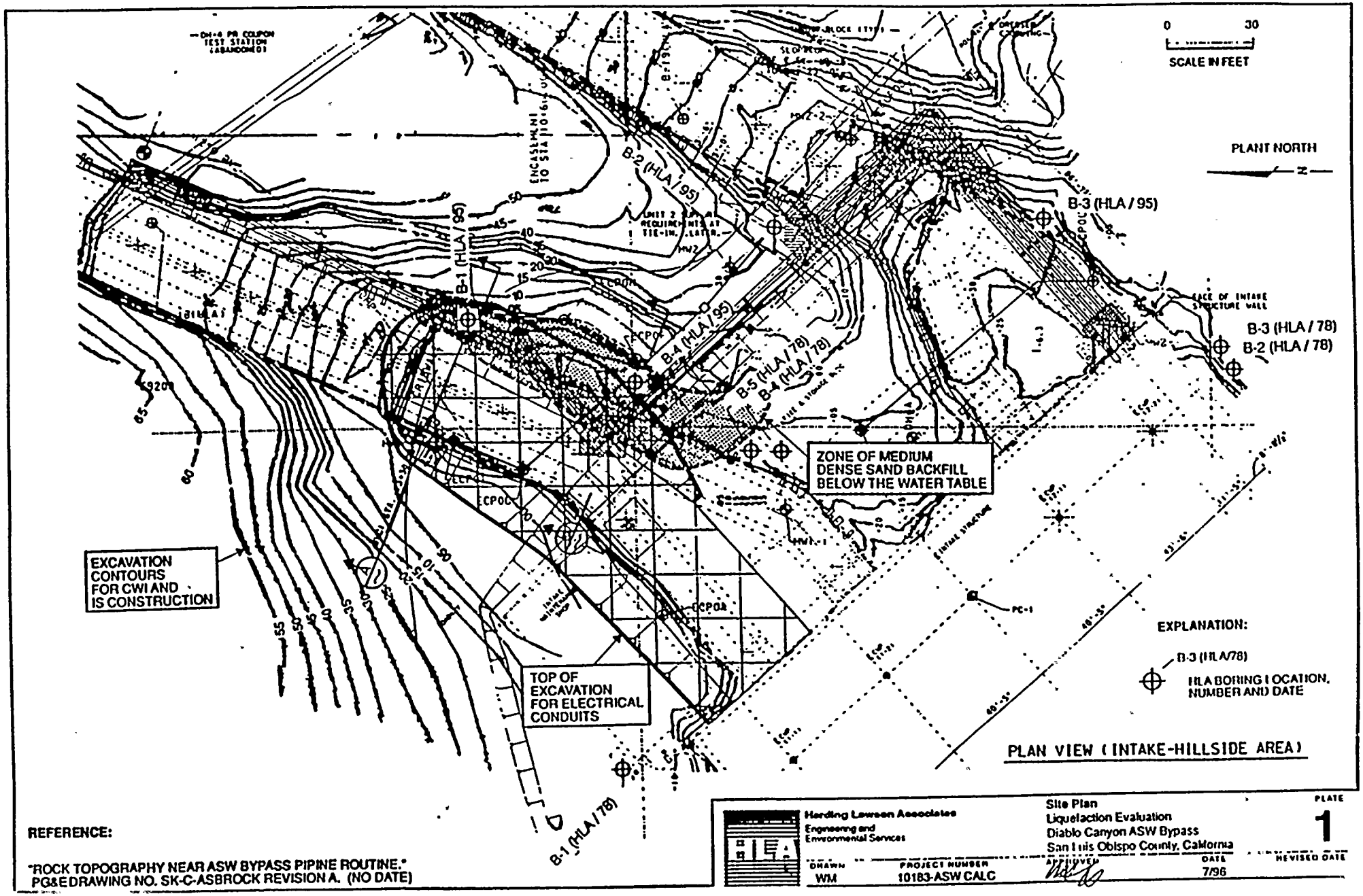

REFERENCE:

"ROCK TOPOGRAPHY NEAR ASW BYPASS PIPINE ROUTINE."
PG&E DRAWING NO. SK-C-ASBROCK REVISION A. (NO DATE)

Harding Lawson Associates
Engineering and Environmental Services

Site Plan
Liquefaction Evaluation
Diablo Canyon ASW Bypass
San Luis Obispo County, California

PLATE 1

DRAWN WM | PROJECT NUMBER 10183-ASW CALC | APPROVED | DATE 7/96 | REVISED DATE

ATTACHMENT NO.2

Calculation Number:10183-96-02
Revision: 0

Preparer: Wayne Magnusen
Checker: Robert Pyke
Date: 7/18/96

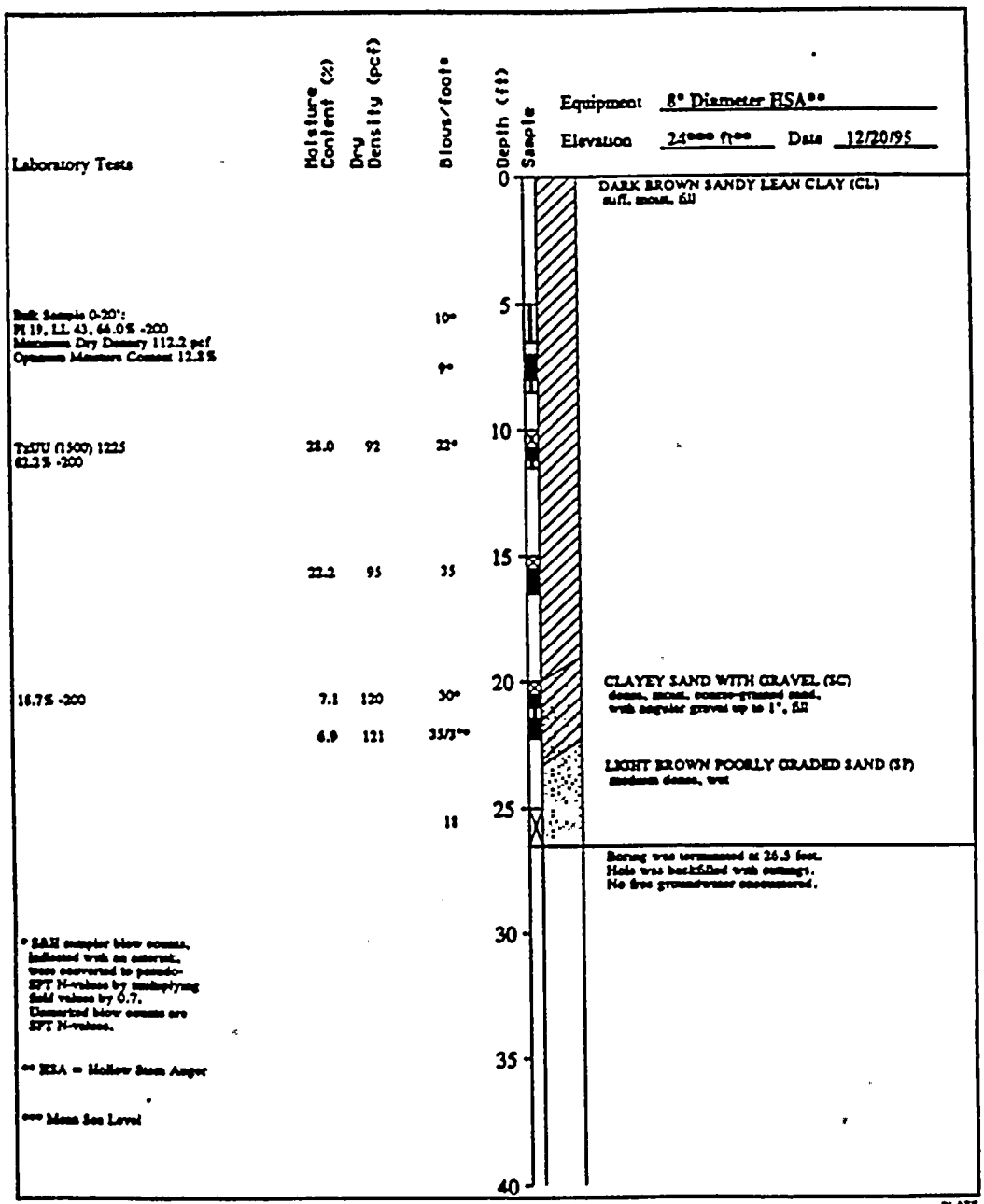

Harding Lawson Associates
Engineering and Environmental Services

Log of Boring B-1 (Sheet 1 of 1)
Diablo Canyon ASW Bypass
San Luis Obispo County, California

PLATE 2

DRAWN	JOB NUMBER	APPROVED	FILE	DATE	REVISED DATE
EO	10183-055		20180G27		

ATTACHMENT NO.3

Calculation Number:10183-96-02
Revision: 0

Preparer: Wayne Magnusen
Checker: Robert Pyke
Date: 7/18/96

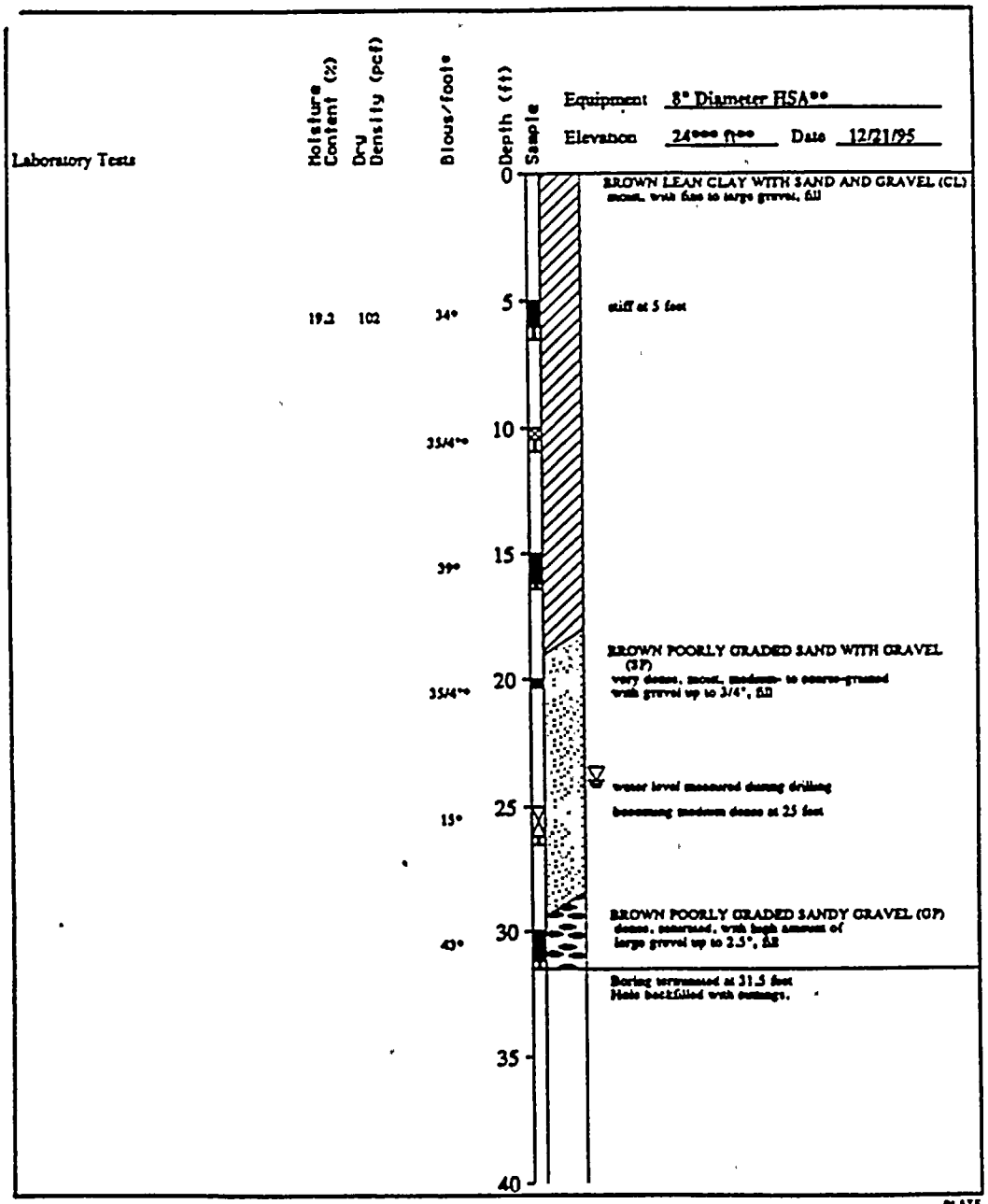

Harding Lawson Associates
Engineering and Environmental Services

Log of Boring B-4 (Sheet 1 of 1)
Diablo Canyon ASW Bypass
San Luis Obispo County, California

PLATE 3

DRAWN	JOB NUMBER	APPROVED	FILE	DATE	REVISED DATE
EO	10183-055		20180G27		

ATTACHMENT NO.4

Calculation Number:10183-96-02
Revision: 0

Preparer: Wayne Magnusen
Checker: Robert Pyke
Date: 7/18/96

Sheet 25 of 27

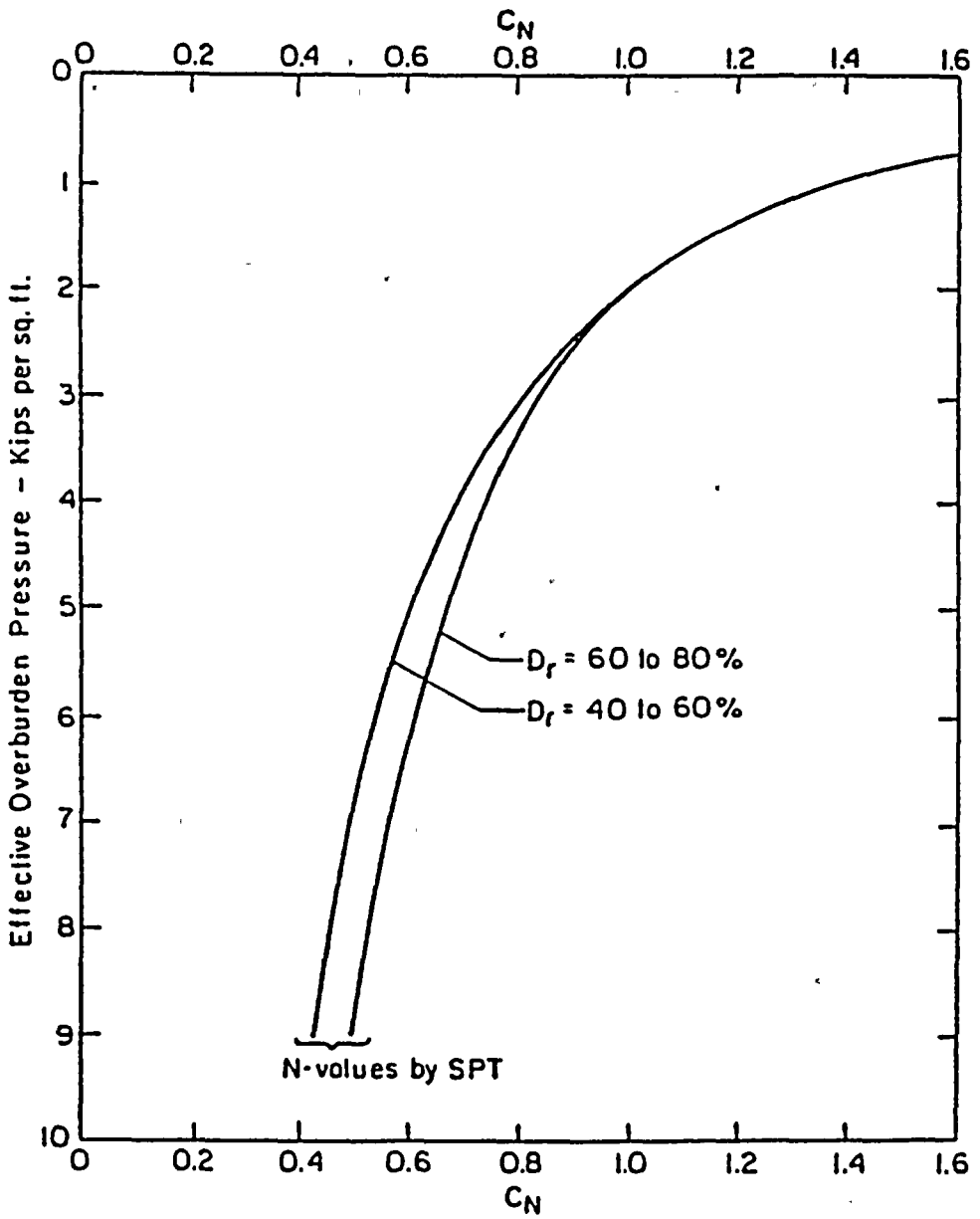

FIG. 3 CURVES FOR DETERMINATION OF C_N

ATTACHMENT NO.5

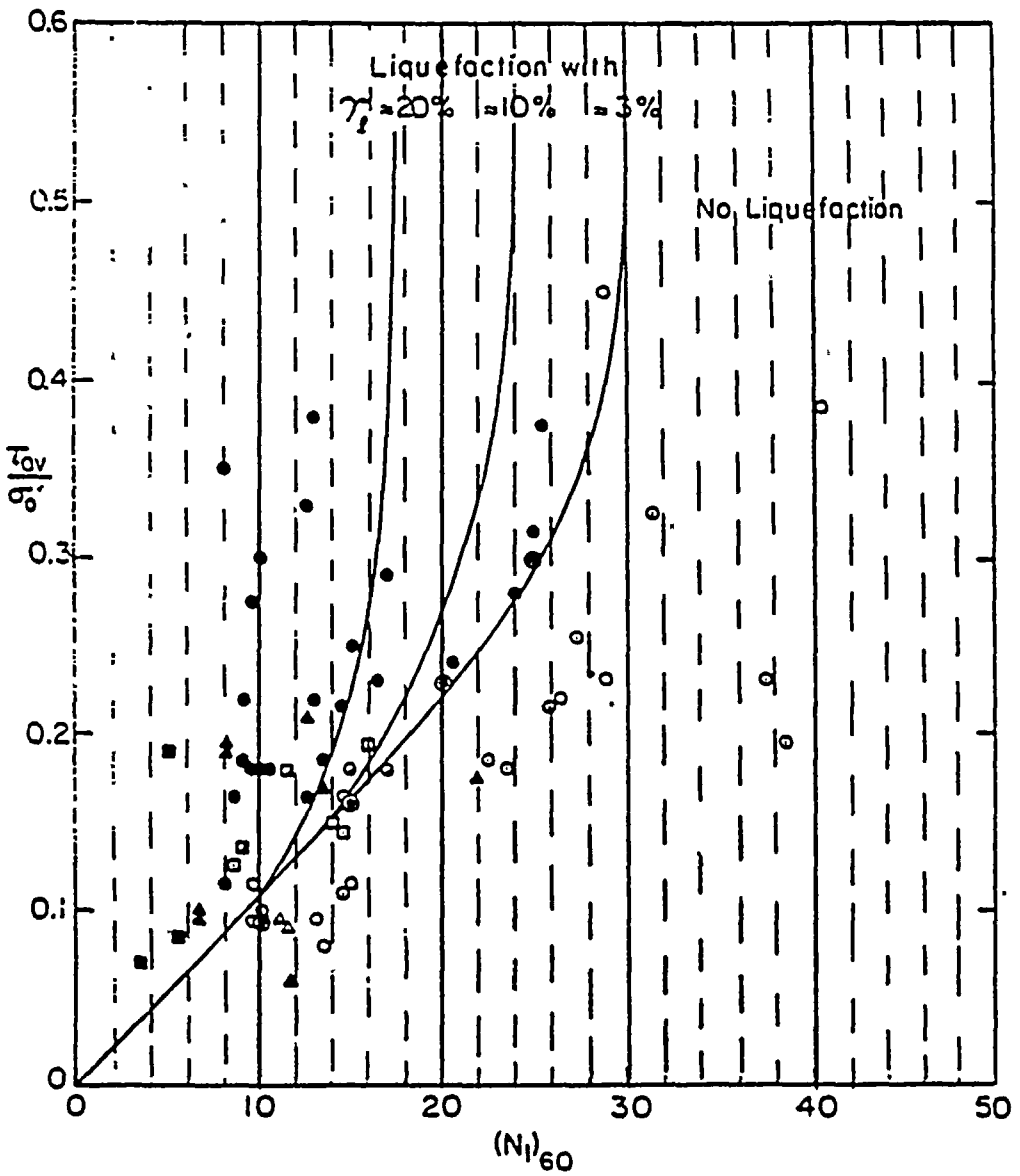

FIG. 13 TENTATIVE RELATIONSHIP BETWEEN CYCLIC STRESS RATIO, N_1-VALUES AND LIMITING STRAINS FOR NATURAL DEPOSITS OF CLEAN SAND

M = 7½

ATTACHMENT NO.6

Preparer: Wayne Magnusen
Checker: Robert Pyke
Date: 7/18/96

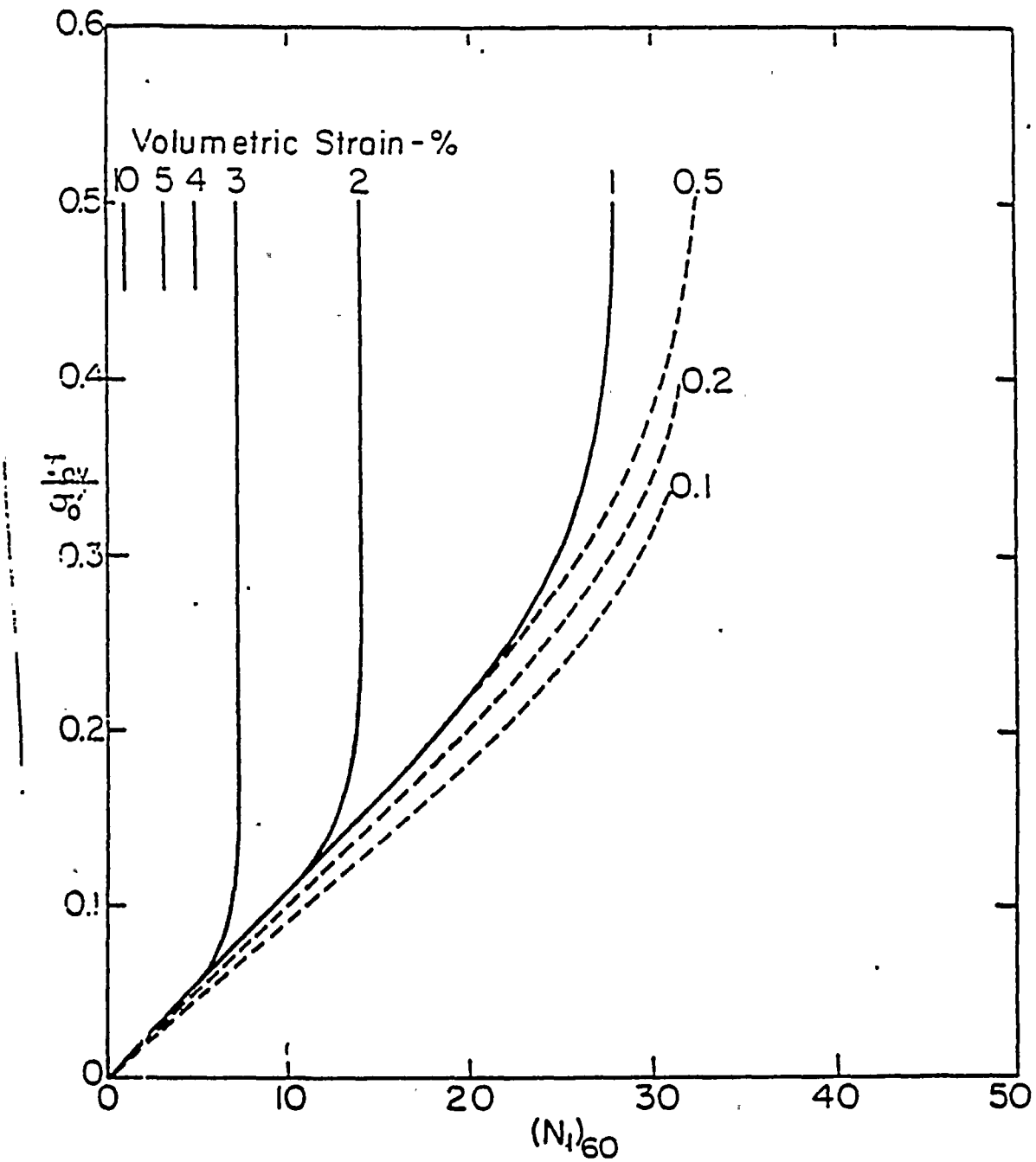

FIG. 6 PROPOSED RELATIONSHIP BETWEEN CYCLIC STRESS RATIO, $(N_1)_{60}$ AND VOLUMETRIC STRAIN FOR SATURATED CLEAN SANDS

Attachment 2.2

. Terzaghi, Karl, Theoretical Soil Mechanics, John Wiley & Sons, Inc., New York, 1943, pages 66 through 76

BOOKS BY TERZAGHI, K. AND PECK, R. B.

Soil Mechanics in Engineering Practice

BOOKS BY TERZAGHI, K.

Theoretical Soil Mechanics

From Theory to Practice in Soil Mechanics

THEORETICAL SOIL MECHANICS

By

KARL TERZAGHI

JOHN WILEY & SONS

New York • Chichester • Brisbane • Toronto

Section B

CONDITIONS FOR SHEAR FAILURE IN IDEAL SOILS

Chapter V

ARCHING IN IDEAL SOILS

18. Definitions. If one part of the support of a mass of soil yield while the remainder stays in place the soil adjoining the yielding part moves out of its original position between adjacent stationary masses of soil. The relative movement within the soil is opposed by a shearing resistance within the zone of contact between the yielding and the stationary masses. Since the shearing resistance tends to keep the yielding mass in its original position, it reduces the pressure on the yielding part of the support and increases the pressure on the adjoining stationary part. This transfer of pressure from a yielding mass of soil onto adjoining stationary parts is commonly called the *arching effect*, and the soil is said to *arch* over the yielding part of the support. Arching also takes place if one part of a yielding support moves out more than the adjoining parts.

Arching is one of the most universal phenomena encountered in soils both in the field and in the laboratory. Since arching is maintained solely by shearing stresses in the soil, it is no less permanent than any other state of stress in the soil which depends on the existence of shearing stresses, such as the state of stress beneath the footing of a column. For instance, if no permanent shearing stresses were possible in a sand, footings on sand would settle indefinitely. On the other hand, every external influence which causes a supplementary settlement of a footing or an additional outward movement of a retaining wall under unchanged static forces must also be expected to reduce the intensity of existing arching effects. Vibrations are the most important influence of this sort.

In the following article two typical cases will be investigated, viz., arching in an ideal sand due to the local yield of a horizontal support and arching in the sand adjoining a vertical support whose lower part yields in an outward direction.

19. State of stress in the zone of arching. The local yield of the horizontal support of a bed of sand shown in Figure 17*a* can be produced by gradually lowering a strip-shaped section *ab* of the support. Before the strip starts to yield, the vertical pressure per unit of area on the horizontal support is everywhere equal to the depth of the layer of sand

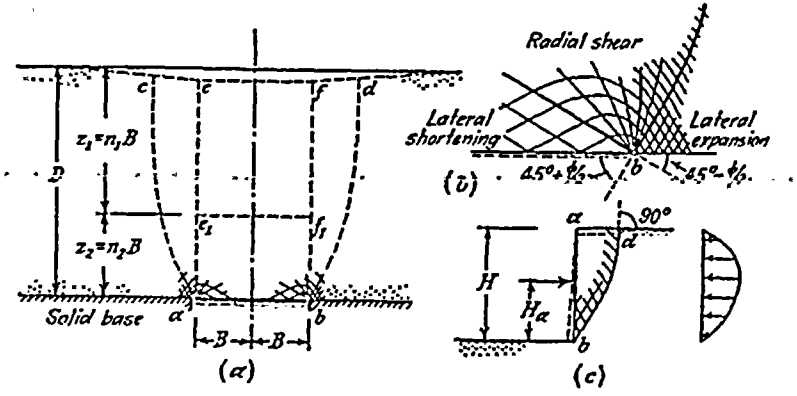

Fig. 17. Failure in cohesionless sand preceded by arching. (*a*) Failure caused by downward movement of a long narrow section of the base of a layer of sand; (*b*) enlarged detail of diagram (*a*); (*c*) shear failure in sand due to yield of lateral support by tilting about its upper edge.

times its unit weight. However, a lowering of the strip causes the sand located above the strip to follow. This movement is opposed by frictional resistance along the boundaries between the moving and the stationary mass of sand. As a consequence the total pressure on the yielding strip decreases by an amount equal to the vertical component of the shearing resistance which acts on the boundaries, and the total pressure on the adjoining stationary parts of the support increases by the same amount. In every point located immediately above the yielding strip the vertical principal stress decreases to a small fraction of what it was before the yield commenced. The total vertical pressure on the base of the layer of sand remains unchanged, because it is always equal to the weight of the sand. Therefore the decrease of the vertical pressure on the yielding strip must be associated with an increase of the vertical pressure on the adjoining parts of the rigid base, involving an abrupt increase of the intensity of the vertical pressure along the edges of the strip. This discontinuity requires the existence of a zone of radial shear comparable to that shown in Figure 15*a*. The radial shear is associated with a lateral expansion of the sand located within the high-pressure zone, on both sides of the yielding strip towards the low-

pressure zone located above the strip. If the base of the layer of sand were perfectly smooth, the corresponding shear pattern should be similar to that indicated in Figure 17*a* and, on a larger scale, in Figure 17*b*.

As soon as the strip has yielded sufficiently in a downward direction, a shear failure occurs along two surfaces of sliding which rise from the outer boundaries of the strip to the surface of the sand. In the vicinity of the surface all the sand grains move vertically downward. This has been demonstrated repeatedly by time-exposure photographs. Such a movement is conceivable only if the surfaces of sliding intersect the horizontal surface of the sand at right angles. When the failure occurs a troughlike depression appears on the surface of the sand as indicated in Figure 17*a*. The slope of each side of the depression is greatest where it intersects the surface of sliding. The distance between these steepest parts of the trough can be measured. It has been found that it is always greater than the width of the yielding strip. Hence, the surfaces of sliding must have a shape similar to that indicated in Figure 17*a* by the lines *ac* and *bd*. The problem of deriving the equations of the surfaces of sliding *ac* and *bd* has not yet been solved. However, experiments (Völlmy 1937) suggest that the average slope angle of these surfaces decreases from almost 90° for low values of $D/2B$ to values approaching $45° + \phi/2$ for very high values of $D/2B$.

The vertical pressure on the lower part of the mass of sand located between the two surfaces of sliding, *ac* and *bd* in Figure 17*a*, is equal to the weight of the upper part reduced by the vertical component of the frictional resistance which acts on the adjoining surfaces of sliding. This transfer of part of the weight of the sand located above the yielding strip onto the adjoining masses of sand constitutes the arching effect.

The preceding reasoning can also be applied to the analysis of the arching effect produced in a mass of sand by the lateral yield of the lower part of a vertical support. In Figure 17*c* the lateral support is represented by *ab*. The surface of the sand is horizontal and the support yields by tilting around its upper edge. After the support has yielded sufficiently, a shear failure occurs in the sand along a surface of sliding *bd* which extends from the foot *b* of the support to the surface of the sand. The stationary position of the upper edge, *a*, of the lateral support prevents a lateral expansion of the upper part of the sliding wedge. Therefore the sand grains located in the upper part of the wedge can move only in a downward direction. Hence the surface of sliding intersects the horizontal surface of the sand at *d* at right angles. The corresponding subsidence of the surface of the sliding wedge is indicated in the figure by a dashed line.

The lateral expansion of the lower part of the sliding wedge is associated with a shortening in a vertical direction. The corresponding subsidence of the upper part of the wedge is opposed by the frictional resistance along the adjoining steep part of the surface of sliding. As a consequence the vertical pressure on the lower part of the wedge is smaller than the weight of the sand located above it. This phenomenon constitutes the arching effect in the sand behind yielding lateral supports whose upper part is stationary.

20. Theories of arching. Most of the existing theories of arching deal with the pressure of dry sand on yielding horizontal strips. They can be divided into three groups. The authors of the theories of the first group merely considered the conditions for the equilibrium of the sand which is located immediately above the loaded strip without attempting to investigate whether or not the results of the computations were compatible with the conditions for the equilibrium of the sand at a greater distance from the strip. The theories of the second group are based on the unjustified assumption that the entire mass of sand located above the yielding strip is in a state of plastic equilibrium.

In the theories of a third group it is assumed that the vertical sections *ae* and *bf* (Fig. 17*a*) through the outer edges of the yielding strip represent surfaces of sliding and that the pressure on the yielding strip is equal to the difference between the weight of the sand located above the strip and the full frictional resistance along the vertical sections (Cain 1916 and others). The real surfaces of sliding, *ac* and *bd* (Fig. 17*a*), are curved and at the surface of the sand their spacing is considerably greater than the width of the yielding strip. Hence the friction along the vertical sections *ae* and *bf* cannot be fully active. The error due to ignoring this fact is on the unsafe side.

The following comments are intended to inform the reader in a general way on the fundamental assumptions of the theories of the first two groups. Engesser (1882) replaced the sand located immediately above the yielding strip by an imaginary arch and computed the pressure on the strip on the basis of the conditions for the equilibrium of the arch. Bierbaumer (1913) compared the sand located immediately above the strip to the keystone in an arch. He assumed that the base of the keystone coincides with the surface of the strip, and that the sides of the keystone are plane and rise from the outer boundaries of the strip towards the center. The pressure on the strip is equal and opposite to the force required to maintain the keystone in its position. Caquot (1934) replaced the entire mass of sand located above the yielding strip by a system of arches. He assumed that the horizontal normal stress in the arches above the center line of the strip is equal to the corresponding vertical normal stress times the flow value N_ϕ, equation 7(4), and he computed the pressure on the strip on the basis of the conditions for the equilibrium of the arches. Völlmy (1937) replaced the curved surfaces of sliding *ac* and *bd* (Fig. 17*a*) by inclined plane surfaces and assumed that the normal stresses on these

surfaces are identical with the normal stresses on similarly oriented sections through a semi-infinite mass of sand in an active Rankine state. The slope of the surfaces of sliding is chosen such that the corresponding pressure on the yielding strip is a maximum. According to the results of some of his investigations an increase of the angle of internal friction of the sand should cause an increase of the pressure on the yielding strip. According to all the other theories and to the existing test results an increase of the angle of internal friction has the opposite effect. Völlmy (1937) also investigated the pressure of the earth on rigid and on flexible culverts and compared the results of his analysis with those obtained by earlier investigators. However, under field conditions the pressure on yielding horizontal supports such as the roofs of culverts or of tunnels depends on many conditions other than those which have been considered so far in theoretical investigations.

All the theories cited above are in accordance with experience in that the pressure on a yielding, horizontal strip with a given width increases less rapidly than the weight of the mass of sand located above the strip and approaches asymptotically a finite value. However, the values furnished by different theories for the pressure on the strip are quite different. In order to find which of the theories deserves preference it would be necessary to investigate experimentally the state of stress above yielding strips and to compare the results with the basic assumptions of the theories. Up to this time no complete investigation of this type has been made, and the relative merit of the several theories is still unknown. The simplest theories are those in the third category which are based on the assumption that the surfaces of sliding are vertical. Fortunately the sources of error associated with this assumption are clearly visible. In spite of the errors the final results are fairly compatible with the existing experimental data. Therefore the following analysis will be based exclusively on the fundamental assumptions of the theories in this category. In connection with a scientific study of the subject Völlmy's publication should be consulted (Völlmy 1937).

If we assume that the surfaces of sliding are vertical as indicated by the lines *ae* and *bf* (Fig. 17*a*) the problem of computing the vertical pressure on the yielding strip becomes identical with the problem of computing the vertical pressure on the yielding bottom of prismatic bins.

For cohesionless materials this problem has been solved rigorously by Kötter (1899). It has also been solved with different degrees of approximation by other investigators. The simplest of the solutions is based on the assumption that the vertical pressure on any horizontal section through the fill is uniformly distributed (Janssen 1895, Koenen 1896). This assumption is incompatible with the state of stress on vertical sections through the soil, but the error due to this assumption is not so important that the assumption cannot be used as a basis for a rough estimate.

Figure 18*a* is a section through the space between two vertical surfaces of sliding. The shearing resistance of the earth is determined by the equation

$$s = c + \sigma \tan \phi$$

The unit weight of the soil is γ and the surface of the soil carries a uniform surcharge q per unit of area. The ratio between the horizontal

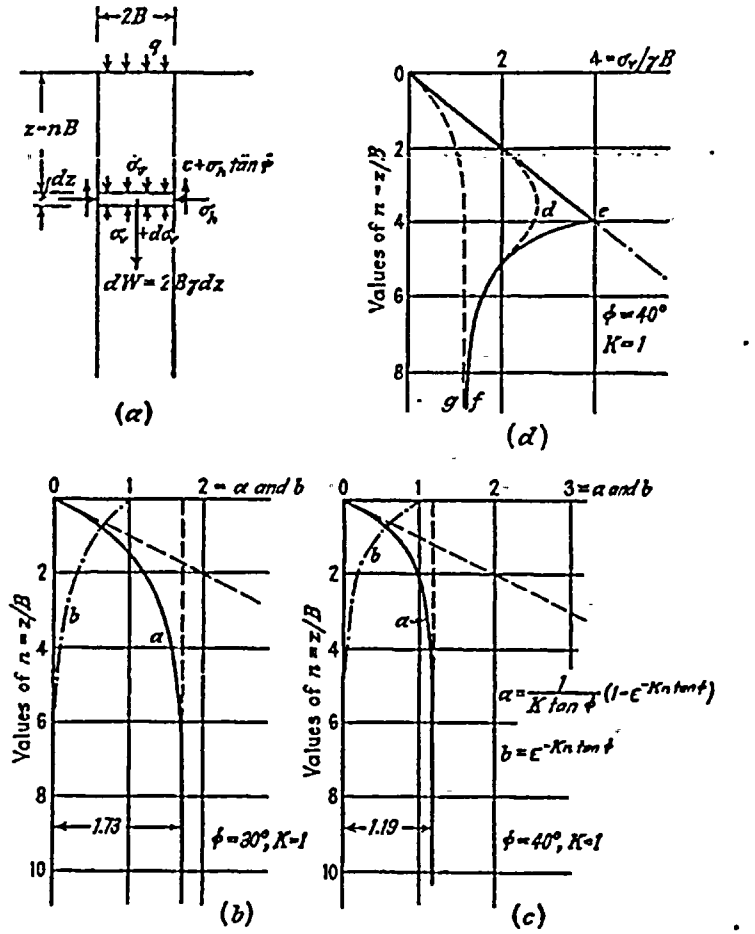

FIG. 18. (*a*) Diagram illustrating assumptions on which computation of pressure in sand between two vertical surfaces of sliding is based; (*c* and *d*) representations of the results of the computations.

and the vertical pressure is assumed to be equal to an empirical constant K at every point of the fill. The vertical stress on a horizontal section at any depth z below the surface is σ_v, and the corresponding normal

stress on the vertical surface of sliding is

$$\sigma_h = K\sigma_v \qquad [1]$$

The weight of the slice with a thickness dz at a depth z below the surface is $2B\gamma\,dz$ per unit of length perpendicular to the plane of the drawing. The slice is acted upon by the forces indicated in the figure. The condition that the sum of the vertical components which act on the slice must be equal to zero can be expressed by the equation

$$2B\gamma\,dz = 2B(\sigma_v + d\sigma_v) - 2B\sigma_v + 2c\,dz + 2K\sigma_v\,dz\tan\phi$$

or

$$\frac{d\sigma_v}{dz} = \gamma - \frac{c}{B} - K\sigma_v\frac{\tan\phi}{B}$$

and

$$\sigma_v = q \quad \text{for} \quad z = 0$$

Solving these equations we obtain

$$\sigma_v = \frac{B(\gamma - c/B)}{K\tan\phi}(1 - \epsilon^{-K\tan\phi\ z/B}) + q\epsilon^{-K\tan\phi\ z/B} \qquad [2]$$

By substituting in this equation in succession the values $c = 0$ and $q = 0$, we obtain

$$c > 0 \quad q = 0 \quad \sigma_v = \frac{B(\gamma - c/B)}{K\tan\phi}(1 - \epsilon^{-K\tan\phi\ z/B}) \qquad [3]$$

$$c = 0 \quad q > 0 \quad \sigma_v = \frac{B\gamma}{K\tan\phi}(1 - \epsilon^{-K\tan\phi\ z/B}) + q\epsilon^{-K\tan\phi\ z/B} \qquad [4]$$

$$c = 0 \quad q = 0 \quad \sigma_v = \frac{B\gamma}{K\tan\phi}(1 - \epsilon^{-K\tan\phi\ z/B}) \qquad [5]$$

If the shearing resistance in a bed of sand is fully active on the vertical sections ae and bf (Fig. 17a), the vertical pressure σ_v per unit of area of the yielding strip ab is determined by equation 5. Substituting in this equation

$$z = nB$$

we obtain

$$\sigma_v = \gamma a B \qquad [6a]$$

wherein

$$a = \frac{1}{K\tan\phi}(1 - \epsilon^{-K\tan\phi\ z/B}) = \frac{1}{K\tan\phi}(1 - \epsilon^{-Kn\tan\phi}) \qquad [6b]$$

For $z = \infty$ we obtain $a = 1/K\tan\phi$ and

$$\sigma_v = \sigma_{v\infty} = \frac{\gamma B}{K\tan\phi} \qquad [7]$$

In Figure 18b the ordinates of the curve marked a represent the values of $n = z/B$ and the abscissas the corresponding values of a for $\phi = 30°$ and $K = 1$, or for $K\tan\phi = 0.58$. Figure 18c contains the same data for $\phi = 40°$ and $K = 1$ or for $K\tan\phi = 0.84$.

Experimental investigations regarding the state of stress in the sand located above a yielding strip (Terzaghi 1936e) have shown that the value K increases from about unity immediately above the center line of the yielding strip to a maximum of about 1.5 at an elevation of approximately $2B$ above the center line. At elevations of more than about $5B$ above the center line the lowering of the strip seems to have no effect at all on the state of stress in the sand. Hence we are obliged to assume that the shearing resistance of the sand is active only on the lower part of the vertical boundaries ae and bf of the prism of sand located above the yielding strip ab in Figure 17a. On this assumption the upper part of the prism acts like a surcharge q on the lower part and the pressure on the yielding strip is determined by equation 4. If $z_1 = n_1B$ is the depth to which there are no shearing stresses on the vertical boundaries of the prism $abfe$ in Figure 17a the vertical pressure per unit of area of a horizontal section e_1f_1 through the prism at a depth z_1 below the surface is $q = \gamma z_1 = \gamma n_1 B$. Introducing this value and the value $z = z_2 = n_2B$ into equation 4 we obtain

$$\sigma_v = \gamma B a_2 + \gamma B n_1 b_2 = \gamma B(a_2 + n_1 b_2) \qquad [8a]$$

wherein

$$a_2 = \frac{1}{K\tan\phi}(1 - \epsilon^{-Kn_2\tan\phi}) \quad \text{and} \quad b_2 = \epsilon^{-Kn_2\tan\phi} \qquad [8b]$$

For $n_2 = \infty$ the value a_2 becomes equal to

$$a_\infty = \frac{1}{K\tan\phi}$$

and the value b_2 equal to zero. The corresponding value of σ_v is

$$= \sigma_{v\infty}\gamma B a_\infty = \frac{\gamma B}{K\tan\phi}$$

which is equal to the value given by equation 7. In other words, the value $\sigma_{v\infty}$ is independent of the depth z_1 in Figure 17a.

The relation between n_2 and a_2 is identical with the relation between

n and a, represented by equation 6*b* and by the plain curves in Figures 18*b* and 18*c*. The relation between the values n and the corresponding values of

$$b = \epsilon^{-Kn\tan\phi}$$

is represented in Figures 18*b* and 18*c* by the dash-dotted curves marked *b*.

In order to illustrate by means of a numerical example the influence of the absence of shearing stresses on the upper part of the vertical sections *ae* and *bf* in Figure 17*a* we assume $\phi = 40°$, $K = 1$, and $n_1 = 4$. Between the surface and a depth $z_1 = n_1 B = 4B$ the vertical pressure on horizontal sections increases like a hydrostatic pressure in simple proportion to depth, as indicated in Figure 18*d* by the straight line *oe*. Below a depth z_1 the vertical pressure is determined by equations 8. It decreases with increasing depth, as shown by the curve *ef* and it approaches asymptotically the value $\sigma_{v\infty}$ (eq. 7).

The dashed line *og* in Figure 18*d* has been plotted on the assumption $n_1 = 0$. The abscissas of this curve are determined by equations 6. With increasing depth they also approach the value $\sigma_{v\infty}$ (eq. 7). The figure shows that the influence of the absence of arching in the upper layers of the bed of sand on the pressure σ_v on a yielding strip practically ceases to exist at a depth of more than about $8B$. Similar investigations for different values of ϕ and of n_1 led to the conclusion that the pressure on a yielding strip is almost independent of the state of stress which exists in the sand at an elevation of more than about $4B$ to $6B$ above the strip (two or three times the width of the strip).

If there is a gradual transition from full mobilization of the shearing resistance of the sand on the lower part of the vertical sections *ae* and *bf* in Figure 17*a* to a state of zero shearing stress on the upper part, the change of the vertical normal stress with depth should be such as indicated in Figure 18*d* by the line *odf*. This line is similar to the pressure curve obtained by measuring the stresses in the sand above the center line of a yielding strip (Terzaghi 1936*e*).

Less simple is the investigation of the effect of arching on the pressure of sand on a vertical support such as that shown in Figure 17*c*. The first attempt to investigate this effect was made on the simplifying assumption that the surface of sliding is plane (Terzaghi 1936*c*). According to the results of the investigation the arching in the sand behind a lateral support with a height H eliminates the hydrostatic pressure distribution and it increases the vertical distance H_a between the point of application of the lateral pressure and the lower edge of the support. The intensity of the arching effect and its influence on the value of the ratio H_a/H depends on the type of yield of the support. If

the support yields by tilting around its lower edge no arching occurs. The distribution of the earth pressure is hydrostatic and the ratio H_a/H is equal to one third. A yield by tilting around the upper edge is associated with a roughly parabolic pressure distribution and the point of application of the lateral pressure is located near midheight. Finally, if the support yields parallel to its original position, the point of application of the lateral pressure may be expected to descend gradually from an initial position close to midheight to a final position at the lower third point. The investigation gave a satisfactory general conception of the influence of the different factors involved, but, owing to the assumption that the surface of sliding is plane, failed to give information regarding the effect of arching on the intensity of the lateral pressure.

In order to obtain the missing information it was necessary to take the real shape of the surface of sliding into consideration. Since the upper edge of the lateral support does not yield, the surface of sliding must intersect the top surface of the backfill at right angles (see Art. 19).

Ohde investigated the influence of this condition on the intensity of the earth pressure on the assumption that the trace of the surface of sliding on a vertical plane is an arc of a circle which intersects the surface of the backfill at right angles (Ohde 1938). The corresponding lateral pressure and the location of the point of application of the lateral pressure have been computed for an ideal sand, with an angle of internal friction $\phi = 31°$, by three different methods.

In one of these, the location of the centroid of the pressure has been determined in such a manner that the stresses along the surface of sliding satisfy Kötter's equation, 17(10). In a second one it has been assumed that the normal stresses on both the wall and the surface of sliding are a function of the second power of the distance from the surface of the backfill, measured along the back of the lateral support and the surface of sliding respectively. The values of the constants contained in the functions have been determined in such a way that the conditions for the equilibrium of the sliding wedge are satisfied. In a third investigation another function has been selected, approximately expressing the distribution of the normal stresses over the boundaries of the sliding wedge. In spite of the differences between the fundamental assumptions, the values obtained by these methods for the ratio between the elevation of the centroid of the earth pressure and the height of the bank range between the narrow limits 0.48 and 0.56. They correspond to an angle of wall friction $\delta = 0$. However, the wall friction was found to have little influence on the location of the centroid of the pressure. Hence we are entitled to assume that the centroid is

located approximately at midheight of the support and the corresponding pressure distribution is roughly parabolic, as shown on the right-hand side of Figure 17c. The investigation has also shown that an increase of the ratio H_a/H due to arching is associated with an increase of the horizontal pressure on the lateral support. A simple method of computing the intensity of the lateral pressure is described in Article 67. It is based on the assumption that the curve of sliding is a logarithmic spiral, which intersects the surface at right angles.

A general mathematical discussion of the influence of the wall movement on the earth pressure has been published by Jáky (1938).

CHAPTER VI

RETAINING WALL PROBLEMS

21. Definitions. Retaining walls are used to provide lateral support for masses of soil. The supported material is called the *backfill*. Figures 19 and 27 represent sections through the two principal types of retaining walls. The wall shown in Figure 19 is called a *gravity wall* because the wall depends on its own weight for stability against the horizontal thrust produced by the lateral earth pressure. On the other hand, the *cantilever retaining wall*, shown in Figure 27, derives part of its stability from the weight of the soil located above the footing at the back of the wall. The side of a retaining wall against which the fill is placed is called the *back of the wall*. The back may be plane or broken, and a plane back may be vertical or inclined (*battered*). The failure of a retaining wall can occur by tilting (*tilting failure*) or by sliding along its base parallel to its original position (*sliding failure*). Either type of failure of the wall is associated with the downward movement of a wedge-shaped body of soil (*abc* in Fig. 19) located immediately back of the wall. This body is called the *sliding wedge*.

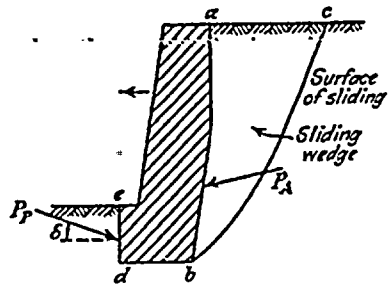

FIG. 19. Earth pressures acting on retaining wall at instant of failure.

22. Assumptions and conditions. Most of the theories of earth pressure are based on the following assumptions: The backfill of the wall is isotropic and homogeneous; the deformation of the backfill occurs exclusively parallel to a vertical plane at right angles to the back of the wall, and the neutral stresses in the backfill material are negligible. Any departure from these fundamental assumptions will be mentioned specifically. In this chapter it will be further assumed that the wall moves to a position which is located entirely beyond the boundary a_1b of the shaded area in Figure 14c. This is the deformation condition.

The width of the shaded area aa_1b in Figure 14c represents the amount by which the horizontal dimensions of the body of sand abc increase while the sand passes from its initial state of stress into that of plastic equilibrium. If a lateral support

Attachment 4.1

Harding Lawson Associates Report, dated 7/3/96, entitled
"Geotechnical Slope Stability Evaluation - ASW System Bypass, Unit 1 -
Diablo Canyon Power Plant - San Luis Obispo County, California"